ISSN: 2639-7536

Research Article

Petroleum and Chemical Industry International

# Numerical Study of Second Law Analysis Using Magnetohydrodynamics on Natural Convection in a Porous Medium with Thermal Radiation and Viscous Dissipation

**Bai Mbye Cham [1,3*], Shams-ul-Islam[1], M. Saleem [2], Dawda Charreh[1,3], Munawwar Ali Abbas[4] and Shaiza Talib[1].**

[1]*Department of Mathematics, COMSATS University Islamabad, Islamabad Campus, Park Road, Tarlai Kalan, Islamabad 45550, Pakistan.*

*2Department of Science and Humanities, Sir Syed CASE Institute of Technology, Islamabad, 44000, Pakistan.*

[3]*Department of Mathematics, University of The Gambia, P.O. Box 3530, Serrekunda, The Gambia. 4Department of Mathematics, University of Baltistan Skardu, Pakistan.*

**[*]Corresponding Author**
Bai Mbye Cham
Department of Mathematics, COMSATS University Islamabad, Islamabad Campus, Park Road, Tarlai Kalan, Islamabad 45550, Pakistan.
Department of Mathematics, University of The Gambia, P.O. Box 3530, Serrekunda, The Gambia.

**Submitted**: 2023, July 23; **Accepted**: 2023, Aug 16: **Published**: 2023, Aug 25

**Citation:** Cham, B. M., Islam, S., Saleem, M., Charreh, D., Abbas, M. A., et al. (2023). Numerical Study of Second Law Analysis Using Magnetohydrodynamics on Natural Convection in a Porous Medium with Thermal Radiation and Viscous Dissipation. *Petro Chem Indus Intern, 6*(4), 296-312.

**Abstract**

*This paper focus on natural convection in the presence of an applied magnetic field for analysing entropy generation and fluid flow phenomena in a porous medium. The numerical technique adopted was the finite difference method. The parameters used for numerically analysing the fluid flows are the Rayleigh number ($103 \leq Ra \leq 106$), Eckert number ($10-6,10-5,5 \times 10-5$) , Forchheimer number ($0 \leq \Gamma \leq 1$), inverse Darcy ($0 \leq \gamma \leq 1$), radiation ($0 \leq Rd \leq 10$), Prandtl number ($Pr = 0.7,1.0,7.0,10$) and Hartmann number ($0 \leq Ha \leq 30$). The numerical results were compared with existing papers and excellent agreements have been made. Findings reveal that as Hartmann increase the streamlines become distorted showing a reduction in the flow rate due to retarding impact of the Lorentz force. Enhancing radiation, leads to the intensification of the flow rate. As Rayleigh number increases entropy generation of the medium significantly increases.*

**Keywords:** Entropy Generation, Magnetohydrodynamics, Natural Convection, Porous Medium, Thermal Radiation.

## 1. Introduction

Magnetic fields and their effects on heat transfer and fluid flows has attracted growing interest in recent years. The behaviors of these flows are generally altered by magnetic fields base on the retarding influences of the Lorentz force, which suppress the fluid flow. Magnetic fields are also used to regulate fluid flows, allowing for precision control, targeted medicine administration, efficient transportation, exact flow measurements, enhanced medical imaging, and unique power generating technologies. Furthermore, its practical applications can be extended to electromagnetic flow-meters, magnetic levitation trains, and magnetic resonance imaging. Numerous developments in magnetohydrodynamics has motivated researchers to investigate applications in this discipline. Ganga et al. studied magnetic effect of viscous and ohmic dissipation on the boundary layer of a fluid through a vertical plate together with heat generation observed internally [1]. The increase on magnetic field strength resulted in higher temperature for the fluid and reduced the thickness of the boundary layer. Geridonmez et al. studied the effects of Hartmann number on temperature distribution. The authors showed that magnetic field has a significant impact on temperature, and as well reduce the rate of heat transfer in the cavity [2]. Subsequently, Fagbade et. al investigated the hydromagnetic effect on thermophoresis and viscous dissipation on fluid-saturated porous media [3]. In a pioneering study, Jamshed et al. model the behavior of non-Newtonian fluids using computational methodologies, taking into consideration viscous dissipation and applied magnetic field. Their research provides a comprehensive investigation of the behavior of magnetic fields and revealing fresh light on the physical principles at work in these systems [4].

Porous media are mostly model by Darcy-Forchheimer which plays a crucial role in many applications. The Darcy-Forchheimer is a frequently used empirical model that represents fluid flow through a porous material by accounting for both the Darcy and

Forchheimer flow components. The model is used to analysed fluid flow in porous materials including soils, rocks, and packed beds. In addition, the Darcy Forcheimer model has practical applications in areas such as geothermal energy, chemical, petroleum and environmental engineering. The knowledge on non-Darcy can help to optimize flow conditions and improve process efficiency in energy systems. For instance, Jumah et al. examined the transfer of heat in saturated porous media using the Darcy-Forchheimer model [5]. The authors concluded that heat transfer in a flow can be improved and optimized by controlling buoyancy and viscous dissipation within the porous cavity. The combined effect of suction and thermal radiation on a non-Darcy flow was studied by Haider et al. [6]. Their investigation revealed that viscous and form drag has a significant effect in the distribution of thermal radiation.

Entropy generation can be found in all heat transfer process due to its irreversible natural process, as stated on the second law of thermodynamics. It is referred to as the qualitative representation of loss of energy in most phenomenon. Many factors contributed greatly to the change in entropy generation in a system, among which includes fluid flow friction, heat transfer mechanisms and hydromagnetic effects. Since entropy concentrate on how much thermal energy is lost in a system. In recent years, extensive research have been done on minimizing the amount of energy lost in thermal systems. Theoretical and experiment research have shown that, the inclusion of magnetic fields can improve heat transfer performance while decreasing system entropy formation. We could observe its wide range of real-life application on boiling water, popcorn making, ice melting and so on [7-11]. Consequently, Khan et al. studied free convection, radiation and generation of entropy on the fluid flows in a Darcy-Forchheimer porous medium and their effects. Rasool et al. analysed entropy generation in a magneto hydronics flow in a porous medium. The authors concluded that regardless of the presence of the solid matrix in the porous medium, entropy generation is significantly hindered by the presences of the magnetic field [12, 13]. Fares et al. investigated the impact of MHD on entropy generation in a Brinkman-Forchheimer porous medium. According to the findings, the magnetic effect has an important influence on entropy generation. Consequently, Tayebs et al. investigated the effects of magnetic fields and entropy generation of natural convective flow in a nanofluid-filled circular enclosure. Bonabid et al. presented a numerical study on the impact of entropy generation in a cavity filled with a binary mixture fluid subjected to thermosolutal convection with imposed magnetic field. The authors performed an extensive analysis of the various factors affecting entropy generation in the system such as heat transfer, viscous dissipation, and magnetic field. Arikoglu et al. analysed the effects of slip on other parameters such as the flow structure and velocity distribution in the system. The paper provide valuable insight into the effects of slip on entropy generation in MHD flows [14-17].

Finite difference method (FDM) is a numerical scheme which discretized domains of equations into grids and using finite difference approximations to estimate the derivatives that appears in the equations under study. It helps in the determination of temperature distributions, heat fluxes, and thermal behaviour in a variety of systems such as heat exchangers, buildings, and electronic devices. FDM's significance as an iterative method stems from its adaptability, precise localized results, iterative convergence, computational efficiency, widespread acceptance, and educational benefits. These characteristics render FDM invaluable for solving various types of partial differential equations (PDEs) and examining fluid dynamics challenges. Al-Odat et al. used FDM to investigate a flat plate exposed to forced convection with an impose magnetic field [18]. The authors investigated the influence of several factors on the entropy production rate, such as magnetic field strength, fluid velocity, and temperature differential. Oztop et al. adopted FDM to analyse fundamental equations of entropy generation and how they relate to the second rule of thermodynamics [19]. With the aid of FDM, Abolbashari et al. discussed the energy lost and irreversibility that occurs in nanofluid flows exposed to magnetic fields over a stretching surface [20]. The governing equations for unsteady flow and heat transfer in a vertical porous channel are numerically solved by Obalalu et al. to visualized temperature and velocity profiles. Similar work was done by Yusuf et al. which focused on radial magnetic fields and viscous dissipation of couette flows [21,22].

An important phenomenon in different fields of study includes natural convection. The impact of which could be notice in the area of environment, geophysics, engineering sciences and industrial systems. They usually occur when fluids are heated below and result to a rise in natural flows. Natural convection influences temperature distribution, fluid dynamics, and entropy generation analyses. Efforts have been made by researchers to understand natural convection phenomena and related domains. Fujii et al. investigated heat transfer on natural convection from a plate with arbitrary inclination [23]. The authors examines the influence of plate inclination on heat transfer characteristics, including the average Nusselt number and boundary layer analysis. A theoretical and experimental study was done by Ostrach et al. on natural convection in an enclosure [24]. Consequently, Bilgen et al. studied the effect of heat transfer on natural convection in an inclined square cavity [25]. Apparently, Shi et al. investigated laminar natural convection heat transfer in a differentially heated square cavity with a thin fin on the relatively hotter wall [26]. The authors examines the effect of fin length and position on flow and heat transfer characteristics, providing insights into the enhancement of heat transfer in such configurations.

Finite difference with Darcy Forchheimer models are investigated in this research. We seek to analysed the effect of entropy generation to properly understand the thermodynamic systems. The results obtained from the study revealed that hydromagnetic and thermal radiation has a significant effect on heat transfer characteristics which leads to changes in entropy generation. The study also has numerous applications in the area of energy conversion and material processing where electromagnetic waves can be used to optimized fluid flows in general.

| Nomenclature | | | |
|---|---|---|---|
| $u$ | velocity along x component | $\rho$ | density |
| $v$ | velocity along y component | $\mu$ | dynamic viscosity |
| $x$ | x component | $C_P$ | specific heat |
| $y$ | y component | $k$ | Thermal conductivity |
| $p$ | Pressure | $K$ | permeability of the porous media |
| $T$ | local temperature | $d$ | mean particle diameter |
| $\epsilon$ | porosity | $F$ | form drag constant |
| $\beta$ | Thermal expansion coefficient | $g$ | gravitational acceleration |
| $\|V\|$ | velocity vector | $\sigma^*$ | Stefan-Boltzmann constant |
| $k'$ | absorption coefficient | $T_h$ | hot area at the boundary |
| $T_c$ | cold area at the boundary | $\omega$ | vortocity |
| $\psi$ | stream function | $\nu$ | Kinematic viscosity |
| $Ra$ | Rayleigh number | $\gamma$ | inverse Darcy number |
| $\Gamma$ | Forchheimer Number | $Gr$ | Grashof Number |
| $Da$ | Darcy number | $Rd$ | radiation parameter |
| $Ec$ | Eckert number | $Nu$ | Local Nusselt number |
| $Nu_{avg}$ | Average Nusselt number | $\alpha$ | Thermal diffusivity |
| $\theta$ | Dimensionless Temperature | $\Phi$ | Viscous dissipation |
| $S_H$ | Entropy due to heat | $S_F$ | Entropy due to fluid friction |
| $S_T$ | Total Entropy | $\Delta\theta$ | Temparature Difference |
| $q_{rx}$ | Radiation flux with respect to x | $q_{ry}$ | Radiation flux with respect to y |
| $q_r$ | Thermal Radiation | $\bar{t}$ | Dimensionless time |
| $\varpi$ | relaxation parameter | $\varrho$ | infinitesimal change |
| $\chi$ | diffusion coeffiecient | $\Upsilon$ | energy in the system |

## 2. Mathematical Formulation

The problem under study is considered unsteady, laminar, incompressible natural convection filled with saturated porous square cavity in the presence of a magnetic field. The geometry of the problem is depicted in figure 1. The top and bottom walls are considered adiabatic, with the left wall considered hot with a temperature of (Th) while the right wall taken as cold and is maintained at relatively lower temperature (Tc). The porous medium is isotropic, homogenous, and the local thermal equilibrium between the fluid and the porous medium exist. The density of buoyancy in the momentum equation is solved on the basis of the Boussinesq model. The thermophysical properties of the flow are assumed as constants. The viscous dissipation, and radiation effects are all inclusive and significant in the Brinkman-Forchheimer model. The following equations are adopted to model the problem stated:

$$\frac{\partial u}{\partial x}+\frac{\partial v}{\partial y}=0 \tag{1}$$

$$\rho\Big(\frac{\partial u}{\partial t}+u\frac{\partial u}{\partial x}+v\frac{\partial u}{\partial y}\Big)=-\frac{\partial p}{\partial x}+\mu\nabla^2 u-\frac{\mu\epsilon^{+}}{K}u-\frac{F\epsilon^{+^2}}{\sqrt{K}}|V|u-\frac{\sigma\beta_0^2}{\epsilon\rho}u \tag{2}$$

$$\rho\Big(\frac{\partial v}{\partial t}+u\frac{\partial v}{\partial x}+v\frac{\partial v}{\partial y}\Big)=-\frac{\partial p}{\partial y}+\mu\nabla^2 v-\frac{\mu\epsilon^{+}}{K}v-\frac{F\epsilon^{+^2}}{\sqrt{K}}|V|v+g\beta(T-T_c) \tag{3}$$

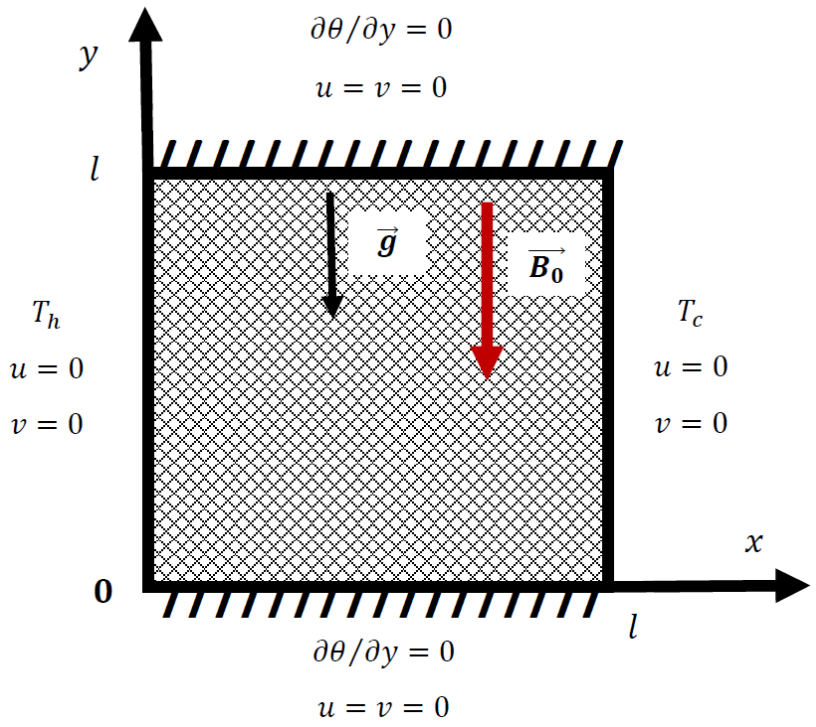


**Figure 1:** The Magnetic Direction, adiabatic process and definitions on the walls

$$\frac{\partial T}{\partial t} + u\frac{\partial T}{\partial x} + v\frac{\partial T}{\partial y} = \frac{k}{\rho c_\rho}\nabla^2 T - \frac{1}{\rho c_\rho}\left[\frac{\partial q_r}{\partial x} + \frac{\partial q_r}{\partial y}\right] + \frac{\mu}{\rho c_\rho K}|V|^2 + \frac{\mu}{\rho c_\rho}\phi + \frac{\sigma\beta_0^2}{\epsilon\rho c_p}u^2 \qquad (4)$$

Here the governing equations (1)-(4) represent the continuity equation, momentum equation in $x$ and $y$ coordinates and the energy equation. We consider ($u$,$v$) as dimensional velocity related components along the ($x$,$y$) Cartesian coordinates. $p$ is the pressure and $T$ the local temperature. The density, dynamic viscosity, specific heat, dimensionless time, and thermal conduction are taken as $\rho$,$\mu$,$c_\rho$,$t$ and $k$ respectively. The radiations terms are $q_{rx} = -\frac{4\sigma^* T_c^3}{3K'}\frac{\partial T^4}{\partial x}$ and $q_{ry} = -\frac{4\sigma^* T_c^3}{3K'}\frac{\partial T^4}{\partial y}$, where $K'$ represents absorption coefficient and $\sigma*$

the Stefan-Boltzmann constant. Using expansion of Taylor series on $T^4$ about $T_c$ and dropping high order terms we

have $T^4 \approx 4TT_c^3 - 3T_c^4$. The magnetic field is considered a $\frac{\sigma\beta_0^2}{\epsilon\rho}$, where $\beta_0$ are the constants impose externally on the magnet and σ is taken as electrically conductive $K = \frac{d^2\epsilon^3}{(150[(1-\epsilon)]^2}$ represents permeability of the cavity, $d$ is the mean particle diameter, $\epsilon$ the porosity. $F = \frac{(1.75(1-\epsilon))}{(d\epsilon^3)}$ is the form drag constant. The norm of the velocity vector taken as $|V| = \sqrt{u^2 + v^2}$, $\beta$

represents the coefficient for thermal expansion and g represents the gravitational acceleration.

The viscous dissipation $\phi$ represents

$$\phi = 2\left[\left(\frac{\partial u}{\partial x}\right)^2 + \left(\frac{\partial v}{\partial y}\right)^2\right] + \left(\frac{\partial v}{\partial x} + \frac{\partial u}{\partial y}\right)^2 \qquad (5)$$

Equation 6 shows the dimensionless parameters

$$X = \frac{x}{H}, \quad Y = \frac{y}{H}, \quad \tau = \frac{\nu}{H^2}t, \quad \theta = \frac{T - T_c}{T_h - T_c}, \quad u = \frac{\nu}{H}U, \quad v = \frac{\nu}{H}V, \quad P = \frac{H^2}{\rho\nu^2}p \qquad (6)$$

We apply the dimensionless parameters given in Eq. (6) to the governing equations (1) to (4) to obtained equations (7) to (10).

$$\frac{\partial U}{\partial X}+\frac{\partial V}{\partial Y}=0 \tag{7}$$

$$\frac{\partial U}{\partial \tau}+U\frac{\partial U}{\partial X}+V\frac{\partial U}{\partial Y}=-\frac{\partial P}{\partial X}+\nabla^2 U-\gamma U-\Gamma|V|U-Ha^2U \tag{8}$$

$$\frac{\partial V}{\partial \tau}+U\frac{\partial V}{\partial X}+V\frac{\partial V}{\partial Y}=-\frac{\partial P}{\partial Y}+\nabla^2 V-\gamma V-\Gamma|V|V+Gr\theta \tag{9}$$

$$\frac{\partial \theta}{\partial \tau}+U\frac{\partial \theta}{\partial X}+V\frac{\partial \theta}{\partial Y}=\frac{1}{Pr}\Big(1+\frac{4}{3}Rd\Big)\nabla^2\theta+\gamma Ec|V|^2+Ec\Phi+Ha^2EcU^2 \tag{10}$$

where $Ra=\dfrac{H^3g\beta(T_h-T_c)}{\alpha\nu}$ represents the Rayleigh, $\gamma=\dfrac{H^2\epsilon^+}{K}$ indicates the inverse darcy, $\Gamma=\dfrac{H^2F\epsilon^{+^2}}{\sqrt{K}}$ is the form drag or Forchheimer, $Gr=\dfrac{Ra}{Pr}$ is the Grashof number and $Pr=\frac{\nu}{\alpha}$ is the Prandtl number. $Da=\dfrac{K}{H^2}$, $Ec=\dfrac{\nu^2}{c_\rho(T_h-T_c)H^2}$, $Ha^2=\dfrac{\sigma\beta_0^2H^2}{\epsilon\mu}$ and $Rd=\frac{4\sigma^*T_c^3}{kK'}$ represents Darcy number, Eckert number, Hartmann number and Radiation respectively. We take $\nabla^2\theta=\Big[\dfrac{\partial^2\theta}{\partial x^2}+\dfrac{\partial^2\theta}{\partial y^2}\Big]$

### 2.1 Vorticity Formulation

For FDM we will use the vorticity formulation approach by multiplying Eq.(2) by $\frac{\partial}{\partial y}$ and Eq.(3) by $\frac{\partial}{\partial x}$, then subtract Eq.(2) from Eq.(3). This will eliminate the pressure term and we will have Eq.(11) as

$$\frac{\partial \omega}{\partial \tau}+u\frac{\partial \omega}{\partial x}+v\frac{\partial \omega}{\partial y}=\nabla^2\omega+Gr\frac{\partial \theta}{\partial x}-(\gamma+\Gamma)\,|V|\,\omega-\Gamma\left(u\frac{\partial|V|}{\partial y}-v\frac{\partial|V|}{\partial x}\right)+Ha^2\frac{\partial u}{\partial y} \tag{11}$$

In terms of the vorticity given as

$$\omega=\frac{\partial v}{\partial x}-\frac{\partial u}{\partial y} \tag{12}$$

A similar approach will be used for the energy equation, but in that case, we will use the stream function ($\psi$) and redefined ($u$,$v$). where

$$u=\frac{\partial \psi}{\partial y}\quad\text{and}\quad v=-\frac{\partial \psi}{\partial x} \tag{13}$$

The vortocity ($\omega$) will then be represented as

$$\frac{\partial^2\psi}{\partial x^2}+\frac{\partial^2\psi}{\partial y^2}=-\omega \tag{14}$$

The energy equation is

$$\frac{\partial \theta}{\partial \tau}+u\frac{\partial \theta}{\partial x}+v\frac{\partial \theta}{\partial y}=\frac{1}{Pr}\Big(1+\frac{4}{3}Rd\Big)\nabla^2\theta+\gamma Ec(u^2+v^2)+Ec\Phi \tag{15}$$

Interms of the stream function

$$\frac{\partial \theta}{\partial \tau}+\frac{\partial \psi}{\partial y}\frac{\partial \theta}{\partial x}-\frac{\partial \psi}{\partial x}\frac{\partial \theta}{\partial y}=\frac{1}{Pr}\Big(1+\frac{4}{3}Rd\Big)\nabla^2\theta+\gamma Ec\left(\left(\frac{\partial \psi}{\partial y}\right)^2+\left(\frac{\partial \psi}{\partial x}\right)^2\right)+Ec\Phi \tag{16}$$

where $\Phi$ is

$$\Phi = \left[4\left(\frac{\partial^2\psi}{\partial x \partial y}\right)^2 + \left(\frac{\partial^2\psi}{\partial y^2} - \frac{\partial^2\psi}{\partial x^2}\right)^2\right] \tag{17}$$

### 2.2 Dimensionless Boundary Conditions

Initial values

$$u = v = \theta = 0 \quad \text{for} \quad t = 0 \qquad\qquad 0 \le x, y \le H.$$

left wall

$$x = 0, \quad \psi = 0, \quad \theta = 1, \quad \omega = -\frac{\partial^2\psi}{\partial x^2}$$

right wall

$$x = 1, \quad \psi = 0, \quad \theta = 0, \quad \omega = -\frac{\partial^2\psi}{\partial x^2}$$

top and bottom walls

$$\psi = 0, \quad \omega = -\frac{\partial^2\psi}{\partial y^2}, \quad \frac{\partial\theta}{\partial y} = 0 \tag{18}$$

## 3. Entropy Generation

Entropy generation is the process through which a system's entropy rises over time. It is a measure of a system's irreversibility. Entropy is connected to the conversion of usable energy into waste or heat and happens in a variety of physical, chemical, and thermodynamic processes. The effect of entropy is frequently related with the second rule of thermodynamics, which states that in ideal circumstances, the total entropy of an isolated system always tends to grow or remain constant. Heat transmission across temperature gradients, fluid friction, chemical reactions, and viscous dissipation processes all contribute to generation of entropy. Eq.(19) to Eq.(21) are the governing equations of entropy with magnet incorporated.

$$S_H = \frac{k}{T_c^2}(\nabla T)^2 - \frac{1}{T_c^2}\left[\frac{\partial q_r}{\partial x} + \frac{\partial q_r}{\partial y}\right] + \frac{\sigma\beta_0^2}{\epsilon T_c}u^2 \tag{19}$$

$$S_F = \frac{\mu}{T_c}\phi + \frac{\mu}{KT_c}|V|^2 \tag{20}$$

Since total entropy is the sum of entropy cause by heat and fluid friction (ST = SH + SF ), Therefore

$$S_T = \frac{k}{T_c^2}(\nabla T)^2 - \frac{1}{T_c^2}\left[\frac{\partial q_r}{\partial x} + \frac{\partial q_r}{\partial y}\right] + \frac{\sigma\beta_0^2}{\epsilon T_c}u^2 + \frac{\mu}{T_c}\phi + \frac{\mu}{KT_c}|V|^2 \tag{21}$$

We apply the dimensionless equation Eq.(6) to the governing equations (19) to (21) to obtained equations (22) to (24)

$$S_H = \left(1 + \frac{4}{3}Rd\right)\left[\left(\frac{\partial\theta}{\partial x}\right)^2 + \left(\frac{\partial\theta}{\partial y}\right)^2\right] + Ha^2\bar{E}cU^2 \tag{22}$$

$$S_F = \bar{E}c\Phi + \gamma\bar{E}c|\mathbf{V}|^2 \tag{23}$$

$$S_T = \left(1 + \frac{4}{3}Rd\right)\left[\left(\frac{\partial\theta}{\partial x}\right)^2 + \left(\frac{\partial\theta}{\partial y}\right)^2\right] + \bar{E}c\Phi + \gamma\bar{E}c|\mathbf{V}|^2 + Ha^2\bar{E}cU^2 \tag{24}$$

where $\Delta\theta = \frac{T_h - T_c}{T_c}$ the dimensionless temperature difference, $\bar{E}c = \frac{PrEc}{\Delta\theta}$ is the modified Eckert, $\Phi$ is the dimensionless viscous dissipation $|\mathbf{V}| = \sqrt{U^2 + V^2}$. We consider $(\Delta T)^2$ as $\left[\left(\frac{\partial T}{\partial x}\right)^2 + \left(\frac{\partial T}{\partial y}\right)^2\right]$.

The Nusselt number is used to measure the ability of a fluid layer to transfer heat more effectively through convection or conduction. The Nusselt's number, a dimensionless quantity, is used to represent heat transfer as seen Eq.(25).

$$\mathrm{Nu} = -\left(1 + \frac{4}{3}Rd\right)\frac{\partial\theta}{\partial x}\Big|_{x=0} \tag{25}$$

Th average nusselts number is also given in Eq.(26) as

$$\mathrm{Nu}_{avg} = \int_0^1 Nudy \tag{26}$$

## 4. Method of Solution

The solutions to the numerical study implemented includes combining buoyancy obtained from Eq.(9) together with Eq.(8) to derive the stream function in Eq.(11). The boundary condition in Eq.(18) where as well applied to the model formulation. The stream function was solved by the successive over relaxation (SOR) with a tolerance of $10^{-5}$. A uniform grid reference of $H$ was adopted where $h = \frac{H}{J-1}$ and $J$(= I) which represents the maximum grid along the ($x$,y) axis. The parameter ($\varpi$) representing relaxation and ($\varrho$) represents the infinitesimal change as the iterations progress

$$\varpi = 2\left[\frac{1-\sqrt{1-\varrho}}{\varrho}\right] \tag{27}$$

where

$$\varrho = \left[\frac{cos\left(\frac{\pi}{i-1}\right) + cos\left(\frac{\pi}{j-1}\right)}{2}\right] \tag{28}$$

The equation for the discretize iterative procedure is given in Eq.(29)

$$\psi_{(i,j)}^{k+1} = \psi_{(i,j}^{k} + \frac{\varpi}{4}\left[\psi_{(i+1,j)}^{k} + \psi_{(i-1,j)}^{k+1} + \psi_{(i,j+1)}^{k} + 4\psi_{(i,j-1)}^{k+1} - \psi_{(i,j)}^{k} - h^2\omega_{(i,j)}^{k}\right] \tag{29}$$

The SOR is repeated between $k$ and $k$+1 until the iteration reach the desired tolerance level and $\omega$ is the vorticity formulation as defined earlier. The new vorticity values at every iteration will be determine by alternative implicit method (ADI). For transient, diffusion, and source components, the *ADI* technique applies forward time central space descretization, whereas the ADI method is changed for convective terms. We use $H = 1$ for the entire calculation. The ADI approach is unconditionally stable. However, the stability of vorticity at the implicit wall borderies, like other implicit approaches, needs a constraint, say $\Delta t$ is taken as time step, and is defined in Eq.(30) as

$$\Delta t \leq \frac{1}{2\chi\left(\frac{2}{h^2}\right) + \frac{|u|+|v|}{h}} \tag{30}$$

where $\chi$ is the coefficient of diffusion term of the equations (transport). However, this time step is restricted for the solid wall boundaries to obtained Eq.(31)

$$\Delta t \leq \frac{h^2}{4\chi} \tag{31}$$

Now the convergence criteria adopted for the model is given in Eq.(32)

$$\left|\frac{\Upsilon_{(i,j)}^{m+1} - \Upsilon_{(i,j)}^{m}}{\Upsilon_{(i,j)}^{m}}\right| \leq 10^{-6} \tag{32}$$

where $m$ denotes the number of time steps and ($i$,$j$) denotes a grid point on the coordinate axes. Y denotes the energy in the system (Saleem et al. [27]).

To validate the proposed code for analyzing entropy generation and fluid flows with an imposed magnetic field in the porous medium. We compared the Grashof number obtained from present work to results by Geridonmez et al. [2]. Table 1 indicates the comparison for $Ha = 0,50,100$, $Gr = 2\times10^4,2\times10^5$ at $Pr = 0.7$. The percentage errors between present and Geridonmez et al. indicate minimal difference guaranteeing the validation of the numerical code adopted [2]. Figure 2 indicates the grid independent study for 31 × 31, 41 × 41, 51 × 51, 71 × 71,81 × 81, 91 × 91 which were compared to the grid adopted for the paper 61 × 61 for fixed parameters of $Ra = 5 \times 10^6, Rd = 2, Ec = 10^{-6}, Pr = 0.7, \gamma = \Gamma = 0.75, Ha = 0$ using vertical velocity at vertical mid plane and horizontal velocity at horizontal mid plane to ensure the accuracy of the results obtained. The reduction in the error calculated solidifies the assumption of the grid independence as shown in figure 2.

| $Gr$ | $Ha$ | Present | [2] | $(\%)Error = \frac{\lvert Gr_{largest} - Gr_{smallest} \rvert}{Gr_{largest}} \times 100$ |
|---|---|---|---|---|
| $2 \times 10^4$ | 0 | 2.5564 | 2.5310 | 0.99 |
| | 50 | 1.0872 | 1.0777 | 0.8 |
| | 100 | 1.0092 | 1.0069 | 0.2 |
| $2 \times 10^5$ | 0 | 5.1233 | 5.0762 | 0.9 |
| | 50 | 2.6590 | 2.6369 | 0.8 |
| | 100 | 1.4492 | 1.4405 | 0.6 |

Table 1: Comparison between Grashof number for present work and Geridonmez et al. [2] for $Pr = 0.7$

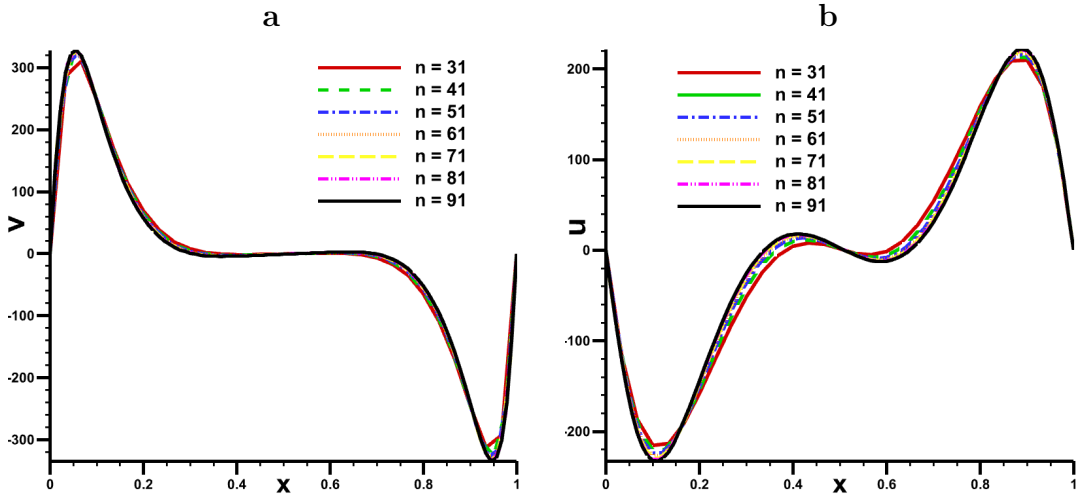


Figure 2: a) Vertical velocity at vertical mid plane, b) Horizontal velocity at horizontal mid plane for $Ra = 5 \times 10^6, Rd = 2, Ec = 10^{-6}, Pr = 0.7, \gamma = \Gamma = 0.75, Ha = 0$

## 5. Results and Discussion

The numerical results shows the effect of factors affecting natural convection fluid flows in a saturated porous square cavity with thermal radiation, viscous dissipation, and an applied magnetic field. The controlling parameter for the numerical study is giving as follows: the Rayleigh number ($10^3 \le Ra \le 10^6$), Eckert number ($10^{-6},10^{-5},5\times10^{-5}$) , Forchheimer number ($0 \le \Gamma \le 10$), inverse Darcy ($0 \le \gamma \le 10$), radiation parameter ($0 \le Rd \le 10$), Prandtl number ($Pr$ = 0.7,1,7,10) and Hartmann number ($0 \le Ha \le 30$). Figures (3-12) shows a study of streamlines, isotherms, isolines of entropy production, local and average Nusselt numbers, and their effects on fluid flow for various dimensionless parameters.

### 5.1 Streamlines, Isotherms and Isolines of Entropy

Figure 3 presence streamlines, isotherms and total entropy for different Hartmann (Ha) numbers with parameters $Ra = 10^5, Pr = 7, Rd = 3, Ec = 10^{-6}, \gamma = \Gamma = 0.75$. In the absences of magnetic field convective core cells are uniformly distribution showing an intensification of convective heat transfer. As $Ha$ increase the streamlines become distorted showing a reduction in the flow rate due to the retarding impact of the Lorentz force. The effects of which could be notice from the values of maximum stream

function which changes from −4.5 to −1.5 as Ha changes from 0 to 30. In addition at $Ha = 30$ the streamlines are displaced along the vertical heated wall. Isotherms depict the temperature distribution and aid in the visualisation of heat transmission patterns. Isotherm behaviour can change in the presence of differing *Ha* number. Higher Hartmann values often restrict fluid mobility due to the magnetic field's dominant impact. As a result, the isotherms become more uniform and nearly parallel, suggesting less convective heat transmission as *Ha* increases. Total entropy is equally affected by the changes in Hartmann number. The thickness of the thermal boundary layer decrease as *Ha* increase. Consequently the entropy generation decrease along the vertical wall as *Ha* grows.

Higher radiation values shows that radiative heat transfer is more dominant. Figure 4 shows effect of different radiation parameters for $Ra = 10^5, Pr = 7, Ha = 30, Ec = 10^{-6}$, and $\gamma = \Gamma = 0.75$. From figure 4, the streamlines are non-uniformly displaced along the heated wall which shows a dominant form of convection when radiation flux is absence. However as radiation increase the streamlines becomes more uniform with smooth circular core in the middle of the cavity. Enhancing radiation, leads to the intensification of the flow rate as the value of the maximum stream function changes from −1.2 to −1.7 when Rd changes from 0 to 10. For isotherms, in the absences of radiation the thermal fields clustered along the left wall. As radiation increases the isotherms are distribution evenly within the cavity. This is because temperature distribution is altered by radiative exchanges between left wall and interior of the cavity. In addition, a nearly thermal stratification is observed for the isotherms at $Rd = 10$, this shows the dominance of conductive heat transfer at high *Rd*. The concentration of isotherms around the vicinity of the vertical walls leads to increase in entropy generation as *Rd* is enhanced (see figure 4).

Figure 5 shows the effect of different Rayleigh number on streamlines , isotherms and isolines of total entropy generation at $Ra = 10^5, Pr = 7, Ha = 30, Ec = 10^{-6}, \gamma = \Gamma = 0.75$. Streamlines appears uniform and more compact at $Ra = 10^3$. At low Ra number conduction is the dominant form of heat transfer. The formation of minor convective cell cores are observed at $Ra = 10^3$. As *Ra* increases convection intensifies due to the buoyancy induce force. Increase in *Ra* changes the formation of the streamlines from a single convective cell core to a double convective cell core regime as depicted in figure 5. The flow strength also increases as the *Ra* increases. The isotherms also appears parallel at $Ra = 10^3$, which shows a thermal stratification at low *Ra* number and rapidly change form as *Ra* changes from $10^3$ to $10^6$. The isotherms becomes more distorted as *Ra* increase due to stronger buoyancy-driven force within the cavity. Rayleigh number has a great impact on the entropy generation. These effects are seen in figure 5. As *Ra* increase the entropy generation of the medium significant increases, this is due to dominance of the convective heat transfer.

### 5.2 Velocity, Total Entropy and Local Nusselt Number

Figure 6 presents the horizontal velocity at the vertical mid plane, total entropy at vertical mid plane and local Nusselt number for different Ha values. From figure 6(a) the horizontal velocity at the vertical mid plane approaches zero. This is attributed to the interaction of the fluid flow structure and temperature difference which leads to an enhancement of the convective heat

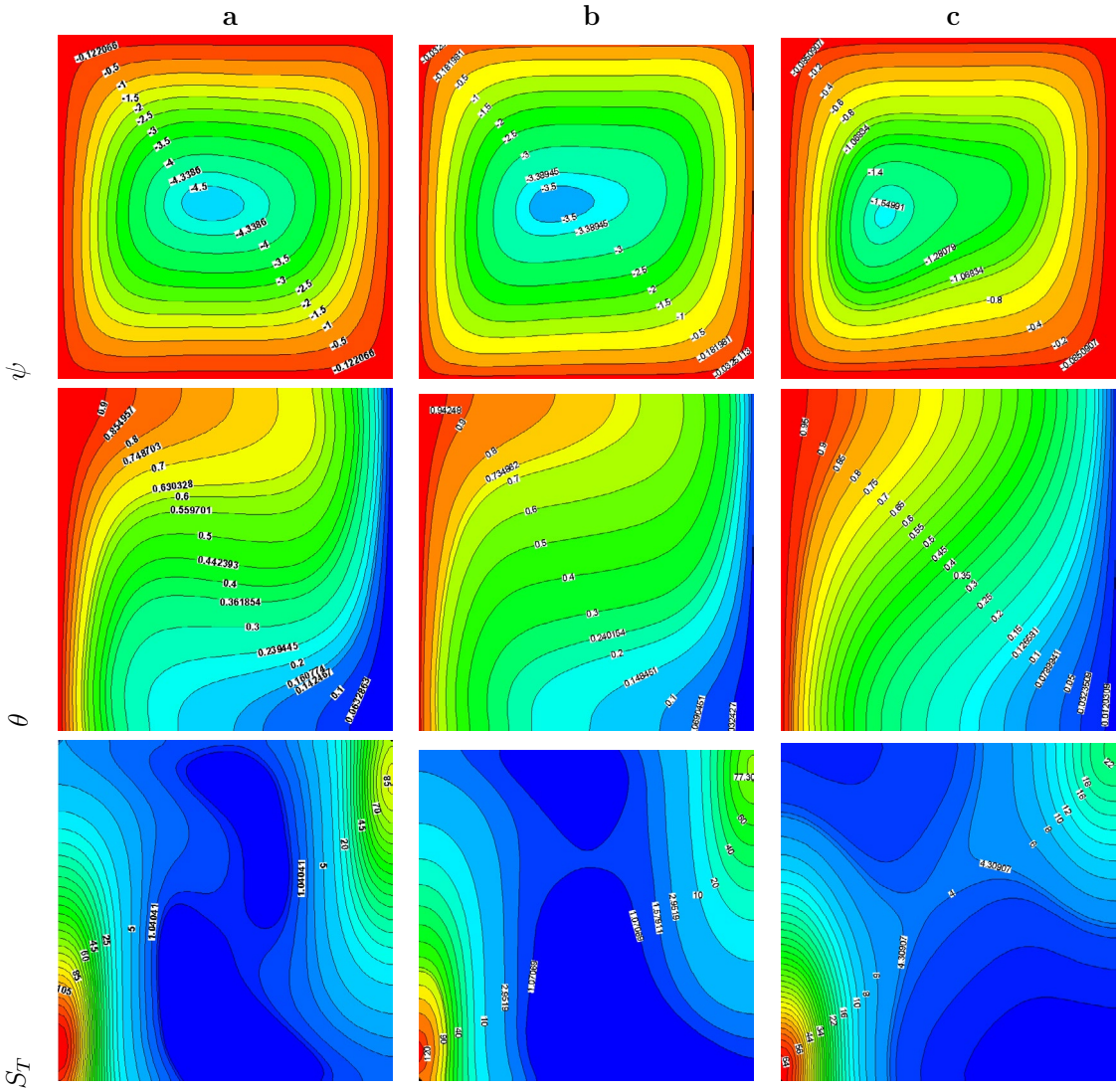


**Figure 3:** Streamlines ($\psi$), Isotherms ($\theta$) and Isolines of Total Entropy Generation $ST$ at $Ra = 10^5, Pr = 7.0, Rd = 3, Ec = 10^{-6}, \gamma = \Gamma = 0.75$ for (a) $Ha = 0$ (b) $Ha = 10$ and (c) $Ha = 30$

transfer. Higher velocities can cause more mixing and fluid agitation, which can contribute to higher irreversibility's and entropy generation. Flow velocity influences flow patterns which in turn influences total entropy generation. The total entropy as presented in figure 6(b) is seen to decrease as Ha increase along the walls of the cavity, with less impact as it moves away from the wall. Total entropy's particular behaviour is determined by the Hartmann number, as well as the flow and heat transfer properties. Higher Nusselt numbers, on the other hand, usually imply improved heat transmission. The flow velocity and temperature gradients, all have an effect on the local Nusselt number. Figure 6 (c) shows that higher Hartmann numbers tend to inhibit flow, resulting in lower local Nusselt numbers due to less convective heat transfer.

Figure 7 shows the horizontal velocity at the vertical mid plane, total entropy at vertical mid plane and local Nusselt number for different Radiation values. Figure 7(a) indicates a smooth

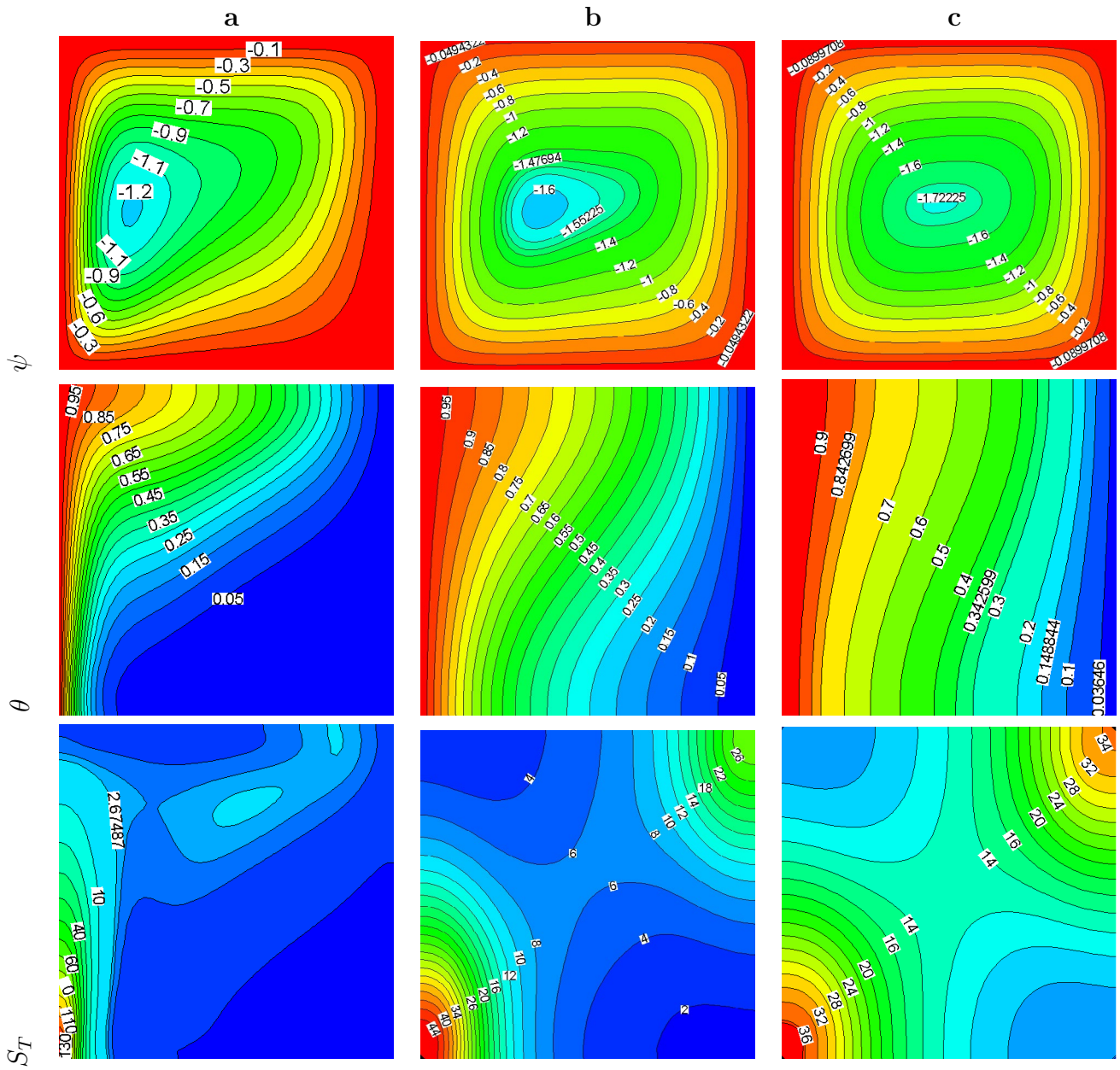


**Figure 4:** Streamlines ($\psi$), Isotherms ($\theta$) and Isolines of Total Entropy Generation $ST$ at $Ra = 10^5, Pr = 7.0, Ha = 30, Ec = 10^{-6}, \gamma = \Gamma = 0.75$ for (a) $Rd = 0$ (b) $Rd = 5$ and (c) $Rd = 10$

flow movements towards zero for the vertical velocity. This is as a result of radiation affecting the velocity profile indirectly by changing the temperature distribution of the fluid, which in turn affects the density and viscosity of the fluid, thereby influencing the flow behaviour. Figure 7(b) depicts the distribution with respect to the total entropy generation profile which combines both the effect of heat transfers and fluid friction as *Rd* varies. Entropy generation could be observed to possessed greater impact along the walls as *Rd* changes positively. Local Nusselt number reduce as *Rd* increase (see figure 7(c)) and this could be attributed to the reduction in the convective heat transfer.

Figure 8 depicted the horizontal velocity at the vertical mid plane, total entropy at vertical mid plane and local Nusselt number for different Rayleigh (*Ra*) values. The Rayleigh number determines the amplitude and distribution of vertical velocities. When the Rayleigh number

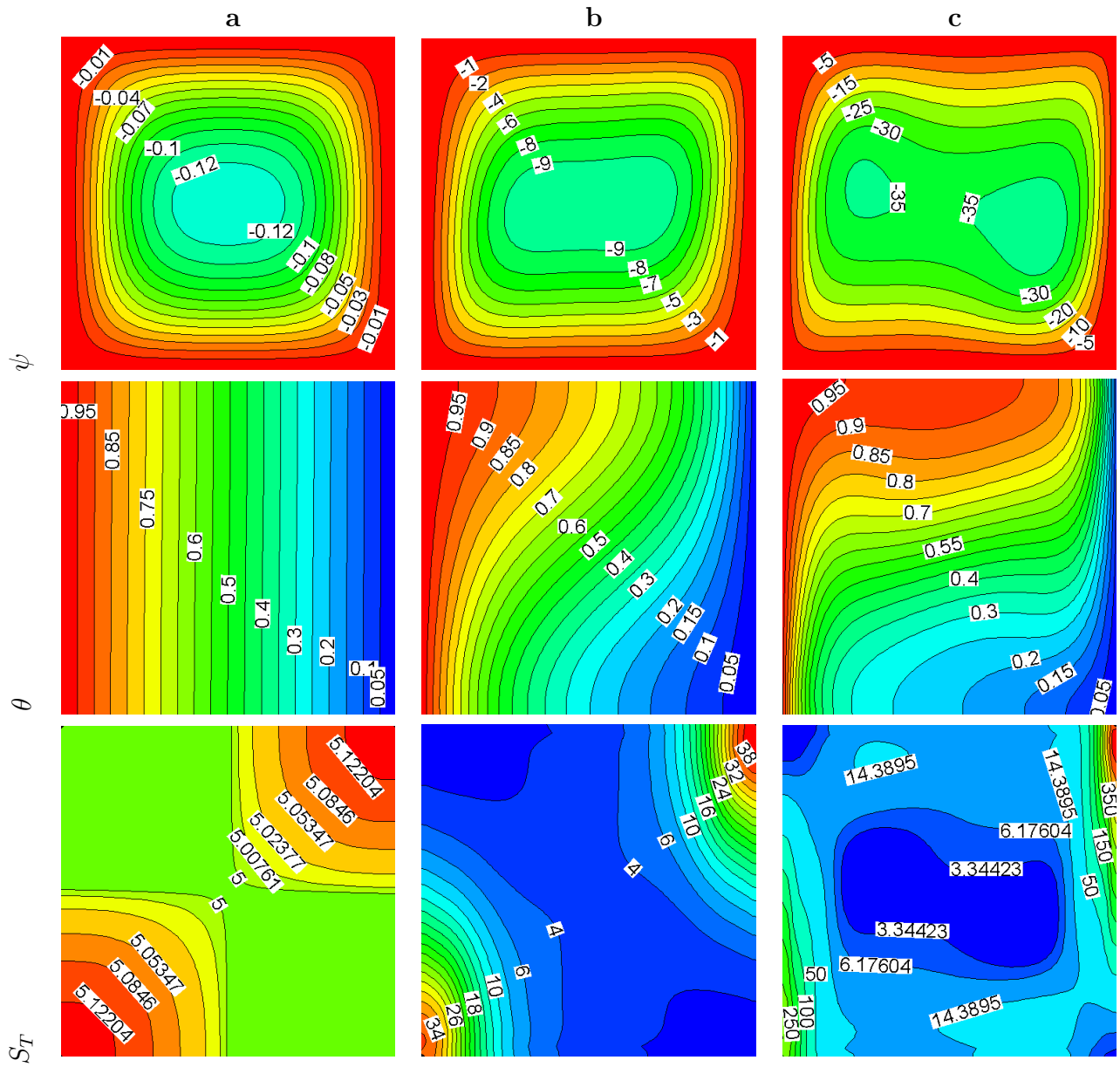


**Figure 5:** Streamlines ($\psi$), Isotherms ($\theta$) and Isolines of Total Entropy Generation $ST$ at $Rd = 3, Pr = 1.0, Ha = 30, Ec = 10{-}6, \gamma = 0.25, \Gamma = 0.5$ for (a) $Ra = 10^3$ (b) $Ra = 10^5$ and (c) $Ra = 10^6$

grows, the buoyancy forces get stronger, causing vertical velocities to increase. Higher Rayleigh numbers result in improved convective heat transfer, resulting in greater upward or downward flow

velocities depending on the temperature gradient as presented in figure 8(a). Convective heat transfer becomes more prominent as the Rayleigh number increases, resulting in improved mixing and heat exchange. This can cause changes in the temperature distribution and the generation of entropy in the flow. We could observed in figure 8(b) that the effect of entropy is generally along the walls of the cavity. The Nusselt number (Nu) is a dimensionless metric that describes the rate of convective heat transport in a fluid. The Rayleigh number has a large influence on the Nusselt number in buoyancy-driven flows. As the Rayleigh number grows, convective heat transmission takes precedence over conductive heat transfer. This causes the Nusselt number to rise as in figure 8(c). Higher Rayleigh numbers correspond to more efficient heat transport and bigger Nusselt numbers.

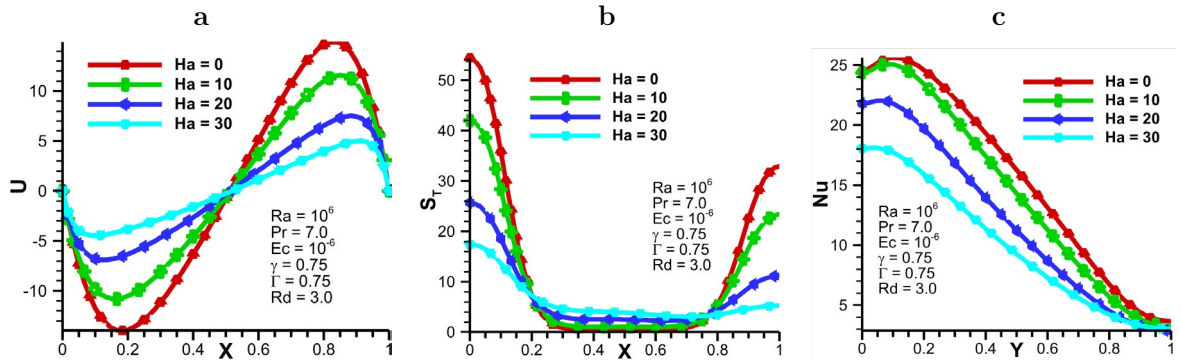


**Figure 6:** (a) Horizontal velocity along the vertical mid plane, (b) Total Entropy at the vertical mid plane and (c) Local Nusselt number at horizontal mid plane

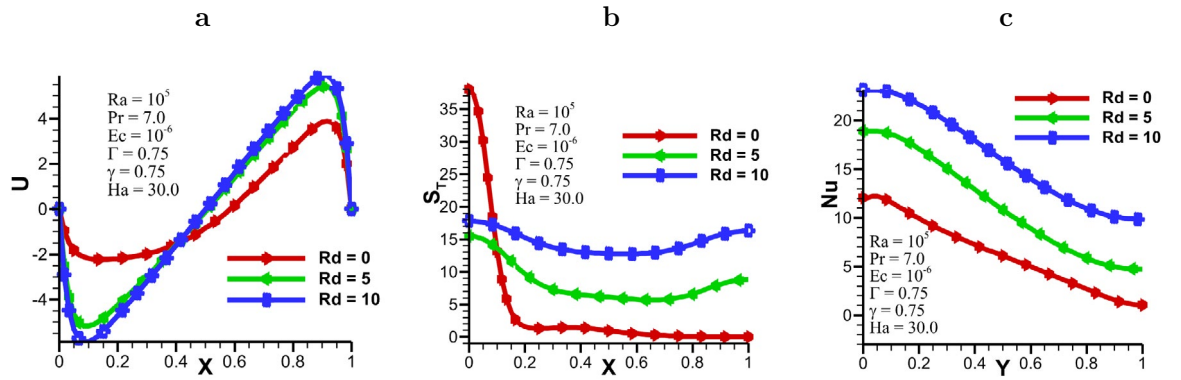


**Figure 7:** (a) Horizontal velocity along the vertical mid plane, (b) Total Entropy at the vertical mid plane and (c) Local Nusselt number at horizontal mid plane

### 5.3 Effect of Time Variation on Maximum Stream Function, Average Nusselt Number and Total Entropy Generation

Figure 9 presence the maximum stream function, average Nusselt number and total entropy generation against time for different Radiation values. The maximum stream function in time dependent flows can alter as the flow patterns change with time. Figure 9(a) shows that as *Rd* increase the maximum stream function increase and the patterns display a smooth movement over time. The uniform nature of the flow pattern over time solidifies the stability assumption of the scheme. Figure 9(b-c) shows the average Nusselt number and total entropy as time evolves. As radiation increase the changes in both cases shows an insignificant effect but maintains the uniform flow.

Figure 10 presence the maximum stream function, average Nusselt number and total entropy generation against time for different Hartmann values. In time-dependent flows, the maximum

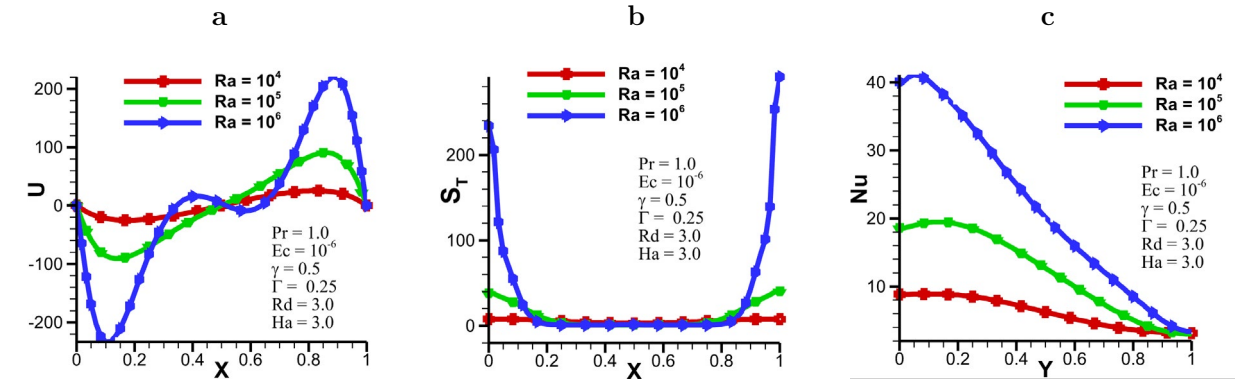


**Figure 8: (a)** Horizontal velocity along the vertical mid plane, (b) Total Entropy at the vertical mid plane and (c) Local Nusselt number at horizontal mid plane

stream function can fluctuate as the flow patterns change over time. The maximum stream function decreases and maintained a smooth pattern over time as *Ha* increases (see figure 10(a)). However a steady flow pattern is observed as time evolves. An insignificant change for different *Ha* values has been observed for both average Nusselt number and total entropy as time evolves (see figure 10(b-c)).

Figure 11 presence the maximum stream function, average nusselt number and total entropy generation against time for different Rayleigh values. The buoyancy forces get greater as the Rayleigh number increases in the flow pattern over time. The maximum stream function increases as *Ra* increases. Figure 11 (a) shows that the flow pattern maintains a steady phenomenon with the stream function as time evolved. The Rayleigh number impact the evolution of the average Nusselt number and total entropy as time passes in buoyancy-driven flows. When the flow begins or when the temperature distribution changes, both the $Nu_{avg}$ and $S_T$ exhibit an insignificant change and a uniform flow pattern exits (see figure 11(b-c)).

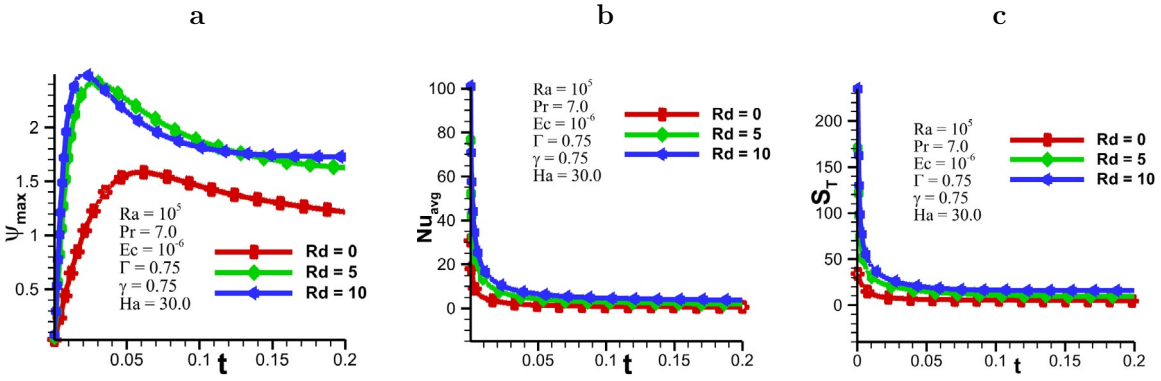


**Figure 9:** (a)Maximum stream function (b) Average Nusselt number and (c) Total entropy

### 5.4 Effect of Form and Viscous drag

The effect of the form and viscous drag forces is presented in figure 12. As the Forchheimer and inverse Darcy increases average Nusselt number increase (see figure 12(a)), while total

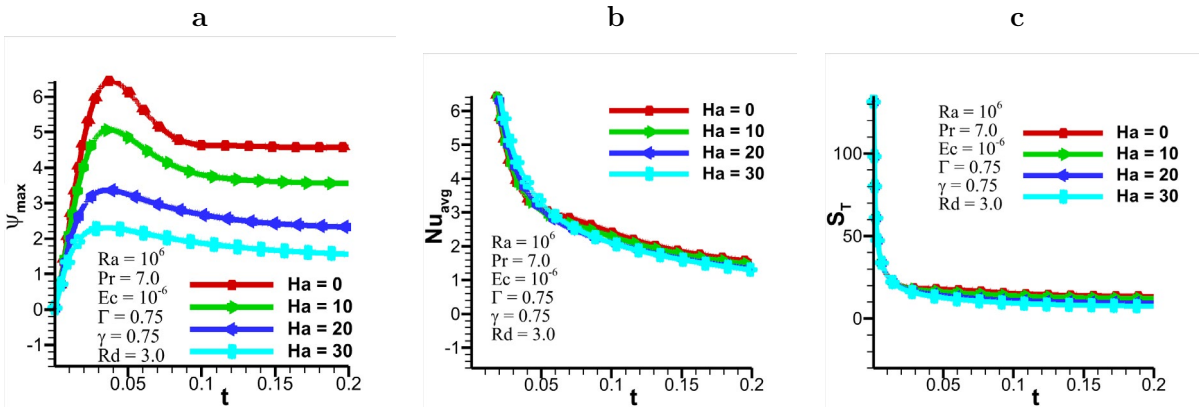


**Figure 10:** (a)Maximum stream function (b) Average Nusselt number and (c) Total entropy

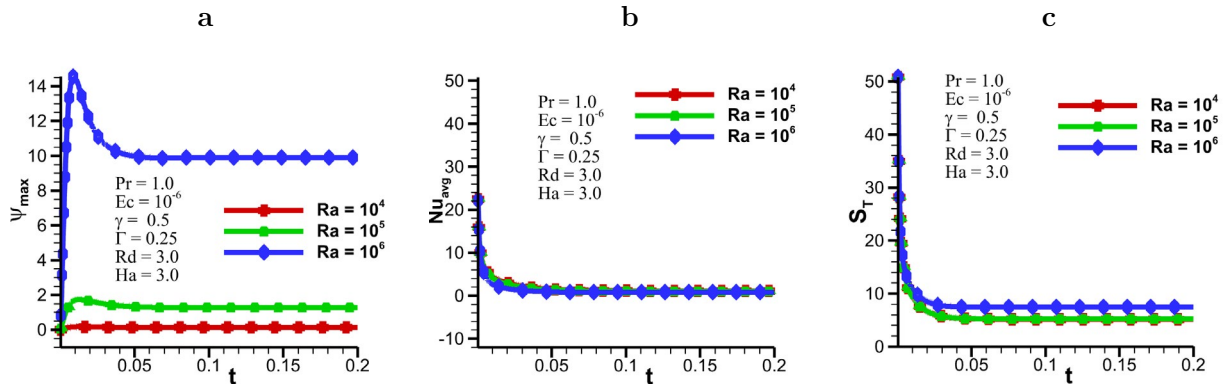


**Figure 11:** (a)Maximum stream function (b) Average Nusselt number and (c) Total entropy

entropy and the maximum stream function diminished for different *Rd* values diminishes (see figure 12(b-c)). The factors affecting average Nusselt number, total entropy and maximum stream function for different Rd values is attributed to the following: A higher emissivity indicates a greater radiative heat transfer. Considering Forchheimer flow resistance and inverse darcy, an increase in emissivity will result in increased heat transfer and reduced temperature gradients within the system. As a result, the temperature-driven entropy formation associated with natural convection will be reduced. More radiation is absorbed with higher absorptivity, resulting in enhanced heat transmission. Higher absorptivity improves heat transmission and change the temperature distribution in the presence of Forchheimer flow resistance. As a result, the creation of entropy may be affected, thereby lowering temperature-driven irreversibility's. When Forchheimer flow resistance is taken into account, scattering and reflection can affect heat transfer patterns and temperature gradients. These temperature distribution variations can have an effect on entropy formation by altering the irreversibility's associated with natural convection. By slowing the flow of fluid around the item, form drag can restrict the maximum stream function. As a result, in the presence of strong form drag, the maximum flow rate and hence the maximum stream function will be reduced. Increased viscous drag is caused by higher viscosity or bigger velocity gradients. Viscous drag has a direct effect on flow and can lower maximum stream function by releasing energy as heat. This drag force resists fluid motion and restricts the maximum flow rate.

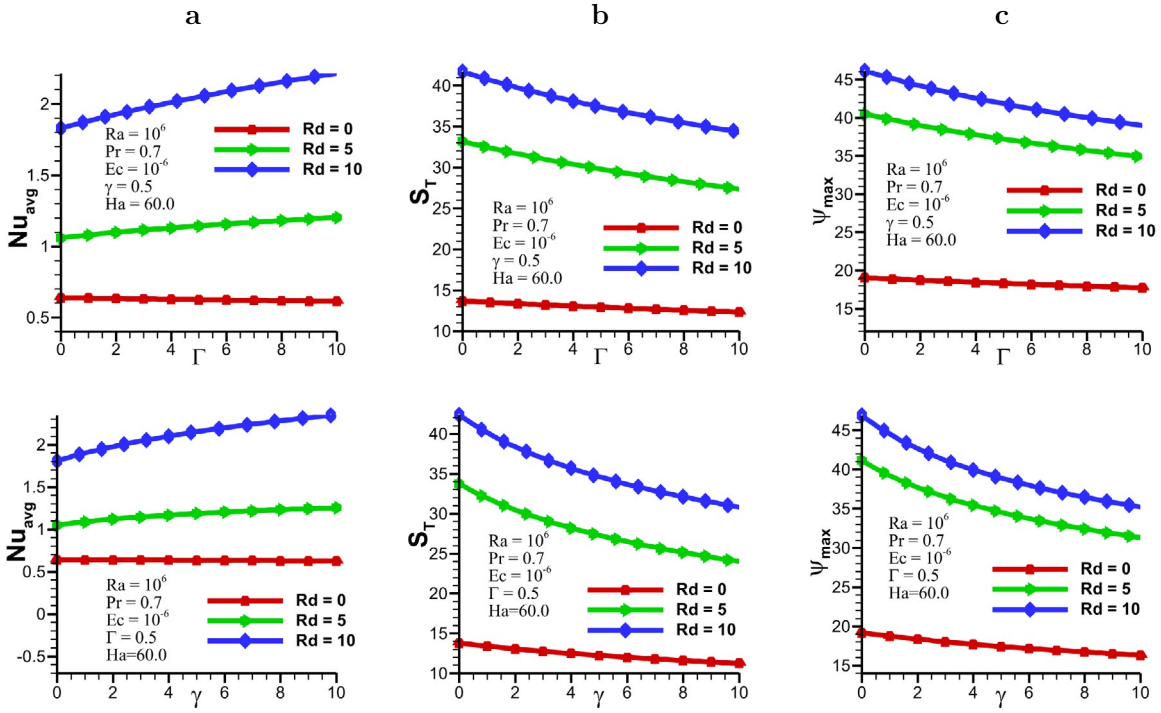


**Figure 12:** (a) Average Nusselt Number at the left wall (b) Total entropy and (c) Maximum stream function

## 6 Conclusions

The investigation of the magnetic effect, Darcy-Forchheimer flows, natural convection, porous medium, and entropy generation has expanded our understanding of fluid flow and heat transfer phenomena. These findings contribute to the advancement of various engineering disciplines, offering opportunities for improved energy efficiency and sustainable development. The inclusion of the radiation effect and the magnetic term in both energy and entropy generation equation has resulted to better analysis of the flow phenomena. The results shown that when Hartmann grows, the streamlines get deformed, causing the flow rate to drop owing to the Lorentz force's retarding impact. The flow rate increases as the radiation level rises. Increases in the Rayleigh number considerably increase the medium's entropy generation. Higher velocities can cause more mixing and fluid agitation, resulting in higher irreversibility's and entropy formation. As time passes, the maximum stream function, average Nusselt number, and total entropy all shows a consistent uniform flow pattern. As Forchheimer and inverse Darcy rise, so does the average Nusselt number, while total entropy and maximum stream function fall.

## References


1. Ganga, B., Ansari, S. M. Y., Ganesh, N. V., & Hakeem, A. A. (2015). MHD radiative boundary layer flow of nanofluid past a vertical plate with internal heat generation/absorption, viscous and ohmic dissipation effects. Journal of the Nigerian Mathematical Society, 34(2), 181-194.
2. Geridonmez, B. P., & Oztop, H. F. (2019). Natural convection in a cavity filled with porous medium under the effect of a partial magnetic field. International Journal of Mechanical Sciences, 161, 105077.
3. Fagbade, A. I., Falodun, B. O., & Boneze, C. U. (2015). Influence of magnetic field, viscous dissipation and thermophoresis on Darcy-Forcheimer mixed convection flow in fluid saturated porous media. American Journal of Computational Mathematics, 5(01), 18-40.
4. Jamshed, W., Gowda, R. J. P., Kumar, R. N., Prasannakumara, B. C., Nisar, K. S., Mahmoud, O., ... & Pasha, A. A. (2022). Entropy production simulation of second-grade magnetic nanomaterials flowing across an expanding surface with viscidness dissipative flux. Nanotechnology Reviews, 11(1), 2814-2826.
5. Jumah, R. Y., Fawzi, A., & Abu-Al-Rub, F. (2001). Darcy-Forchheimer mixed convection heat and mass transfer in fluid saturated porous media. International Journal of Numerical Methods for Heat & Fluid Flow, 11(6), 600-618.
6. Haider, F., Hayat, T., & Alsaedi, A. (2021). Flow of hybrid nanofluid through Darcy-Forchheimer porous space with variable characteristics. Alexandria Engineering Journal, 60(3), 3047-3056.
7. Saleem, M., Hossain, M. A., Mahmud, S., & Pop, I. (2011). Entropy generation in Marangoni convection flow of heated fluid in an open ended cavity. International Journal of Heat and Mass Transfer, 54(21-22), 4473-4484.
8. Sciacovelli, A., Verda, V., & Sciubba, E. (2015). Entropy generation analysis as a design tool—A review. Renewable and Sustainable Energy Reviews, 43, 1167-1181.
9. Shojaeian, M., & Koşar, A. (2014). Convective heat transfer and entropy generation analysis on Newtonian and non-Newtonian fluid flows between parallel-plates under slip boundary conditions. International Journal of Heat and Mass Transfer, 70, 664-673.
10. Kiyasatfar, M. (2018). Convective heat transfer and entropy generation analysis of non-Newtonian power-law fluid flows in parallel-plate and circular microchannels under slip boundary conditions. International Journal of Thermal Sciences, 128, 15-27.
11. Zeeshan. (2022). Second law and entropy generation analysis of magnetized viscous fluid flow over a permeable expandable sheet with nonlinear thermal radiation: Brownian and thermophoresis effect. Advances in Mechanical Engineering, 14(1), 16878140221075295.
12. Khan, M. I., & Alzahrani, F. (2021). Free convection and radiation effects in nanofluid (Silicon dioxide and Molybdenum disulfide) with second order velocity slip, entropy generation, Darcy-Forchheimer porous medium. International Journal of Hydrogen Energy, 46(1), 1362-1369.
13. Rasool, G., Shafiq, A., Khan, I., Baleanu, D., Sooppy Nisar, K., & Shahzadi, G. (2020). Entropy generation and consequences of MHD in Darcy–Forchheimer nanofluid flow bounded by non-linearly stretching surface. Symmetry, 12(4), 652.
14. Fares, R., Mebarek-Oudina, F., Aissa, A., Bilal, S. M., & Öztop, H. F. (2021). Optimal entropy generation in Darcy-Forchheimer magnetized flow in a square enclosure filled with silver based water nanoliquid. Journal of Thermal Analysis and Calorimetry, 1-11.
15. Tayebi, T., Dogonchi, A. S., Karimi, N., Ge-JiLe, H., Chamkha, A. J., & Elmasry, Y. (2021). Thermo-economic and entropy generation analyses of magnetic natural convective flow in a nanofluid-filled annular enclosure fitted with fins. Sustainable Energy Technologies and Assessments, 46, 101274.
16. Bouabid, M., Hidouri, N., Magherbi, M., & Brahim, A. B. (2011). Analysis of the magnetic field effect on entropy generation at thermosolutal convection in a square cavity. Entropy, 13(5), 1034-1054.
17. Arikoglu, A., Ozkol, I., & Komurgoz, G. (2008). Effect of slip on entropy generation in a single rotating disk in MHD flow. Applied Energy, 85(12), 1225-1236.
18. Al-Odat, M. Q., Damseh, R. A., & Al-Nimr, M. (2004). Effect of magnetic field on entropy generation due to laminar forced convection past a horizontal flat plate. Entropy, 6(3), 293-303.
19. Oztop, H. F., & Al-Salem, K. (2012). A review on entropy generation in natural and mixed convection heat transfer for energy systems. Renewable and Sustainable Energy Reviews, 16(1), 911-920.
20. Abolbashari, M. H., Freidoonimehr, N., Nazari, F., & Rashidi, M. M. (2014). Entropy analysis for an unsteady MHD flow past a stretching permeable surface in nano-fluid. Powder Technology, 267, 256-267.
21. Obalalu, A. M., Wahaab, F. A., & Adebayo, L. L. (2020). Heat

transfer in an unsteady vertical porous channel with injection/suction in the presence of heat generation. Journal of Taibah University for Science, 14(1), 541-548.
22. Yusuf, T., & Oni, M. (2018). Entropy generation under the influence of radial magnetic field and viscous dissipation of generalized Couette flow in an annulus. Propulsion and Power Research, 7(4), 342-352.
23. Fujii, T., & Imura, H. (1972). Natural-convection heat transfer from a plate with arbitrary inclination. International journal of heat and mass transfer, 15(4), 755-767.
24. Ostrach, S. (1972). Natural convection in enclosures. In Advances in heat transfer (Vol. 8, pp. 161-227). Elsevier.
25. Bilgen, E., & Oztop, H. (2005). Natural convection heat transfer in partially open inclined square cavities. International Journal of Heat and Mass Transfer, 48(8), 1470-1479.
26. Shi, X., & Khodadadi, J. M. (2003). Laminar natural convection heat transfer in a differentially heated square cavity due to a thin fin on the hot wall. J. Heat Transfer, 125(4), 624-634.
27. Saleem, M., Hossain, M. A., & Saha, S. C. (2014). Double diffusive Marangoni convection flow of electrically conducting fluid in a square cavity with chemical reaction. Journal of heat transfer, 136(6), 062001.